International Journal of Heat and Mass Transfer 52 (2009) 1185–1192

Contents lists available at ScienceDirect

International Journal of Heat and Mass Transfer

journal homepage: www.elsevier.com/locate/ijhmt

Analysis for the dual-phase-lag bio-heat transfer during magnetic hyperthermia treatment

Kuo-Chi Liu [a,*], Han-Taw Chen [b]

[a] Department of Mechanical Engineering, Far East University, 49 Chung Hua Road, Hsin-Shih, Tainan 744, Taiwan, ROC
[b] Department of Mechanical Engineering, National Cheng Kung University, Tainan 701, Taiwan, ROC

ARTICLE INFO

Article history:
Received 29 July 2008
Received in revised form 22 August 2008
Available online 30 October 2008

ABSTRACT

Magnetic fluid hyperthermia is one of hyperthermia modalities for tumor treatment. The control of temperatures is necessary and important for treatment quality. Living tissue is highly non-homogenous, and the velocity of heat transfer in it should be limited. Thus, this work analyzes the temperature rise behaviors in biological tissues during hyperthermia treatment within the dual-phase-lag model, which accounts the effect of local non-equilibrium on the thermal behavior. A small tumor surrounded by the health tissue is considered as a solid sphere. The influences of lag times, metabolic heat generation rate, blood perfusion rate, and other physiological parameters on the thermal response in tissues are investigated. While the metabolic heat generation takes little percentage of heating source, its effect on the temperature rise can be ignored. The control of the blood perfusion rate is helpful to have an ideal hyperthermia treatment. The lag times, τ_q and τ_T, affect the bio-heat transfer at the early times of heating. The total effect of τ_q and τ_T on the bio-heat transfer may be different for the same τ_T/τ_q value.

1. Introduction

Cancer cells have a higher chance of dying when the temperature is above 42.5 °C, and the rate of death drastically increases with increasing temperature [1]. Magnetic fluid hyperthermia is one of hyperthermia modalities for tumor treatment. In magnetic tumor hyperthermia, fine magnetic particles are localized at the tumor tissue. Then, an alternating magnetic field is applied to the target region, which heats the magnetic particles by magnetic hysteresis losses. These particles might act as localized heat sources. An ideal hyperthermia treatment should selectively destroy the tumor cells without damaging the surrounding healthy tissue. Moroz et al. [2] stated that magnetic fluid hyperthermia had the maximum potential for such selective targeting. It was absolutely a necessity for hyperthermia treatment planning to understand the heat transport occurring in biological tissues [3]. Especially, the temperature distribution inside as well as outside the target region must be known as function of the exposure time in order to provide a level of therapeutic temperature and, on the other hand, to avoid overheating and damaging of the surrounding healthy tissue .

Several papers [4–8] have studied the behavior of bio-heat transfer in multi-layer living tissues during hyperthermia treatment with the Pennes' equation. Andrä et al. [4] modeled small breast carcinomas surrounded by extended health tissue as a solid sphere with constant heat generation. They gave an elementary solution of the original heat conduction problem without the effects of blood perfusion and metabolism. Bagaria and Johnson [5] considered the tissue model as two finite concentric spherical regions with the blood perfusion effect and presented analytical and numerical solutions to the model with the mixed boundary conditions. Maenosono and Saita [6] carried out theoretical assessment of FePt magnetic nanoparticles as heating elements for hyperthermia. The temperature rise behavior *in vivo* with the Neuman boundary conditions in spherical co-ordinates was estimated. Durkee et al. [7] offered the exact solutions to the Pennes' bio-heat equation in one-dimensional multi-layer spherical geometry. Tsuda et al. [8] developed an inverse method to optimize the heating conditions during a hyperthermia treatment.

It was well known that the Pennes' equation was based on the classical Fourier's law that depicted an infinitely fast propagation of thermal signal. In reality, accumulating enough energy to transfer to the nearest element would take time in the process of heat transfer. The literatures [9–11] reported the relaxation time in biological bodies to be 20–30 s. Mitra et al. [12] found the relaxation time for processed meat is of the order of 15 s. The experimental investigation made by Roetzel et al. [13] showed the value of relaxation time about 2 s for processed meat. The above literatures further supported the phenomenon of finite thermal propagation velocity in the process of bio-heat transfer. Since the concept of finite heat propagation velocity received the attention from relevant researchers [14–17], the paradox occurred in the classical heat transfer model was solved. Although the thermal wave model

* Corresponding author.
E-mail addresses: kuochi.liu@msa.hinet.net, kcliu@cc.feu.edu.tw (K.-C. Liu).

0017-9310/$ - see front matter © 2008 Elsevier Ltd. All rights reserved.
doi:10.1016/j.ijheatmasstransfer.2008.08.025

Nomenclature

a	length of tissue, m
c	specific heat of tissue, J/kg K
c_b	specific heat of blood, J/kg K
f	parameter defined in Eq. (21)
H	new dependent variable, $H = r(T - T_i)$
$\tilde{H}$	Laplace transform of H
k	thermal conductivity, W/m K
K	parameter defined in Eq. (22)
ℓ	distance between two neighboring nodes, m
n	total number of nodes
P	power density, W/m^3
q_m	metabolic heat generation, W/m^3
q_r	spatial heating source, W/m^3
r	space coordinate, m
R	radius of tumor, m
s	Laplace transform parameter
t	time, s
T	temperature of tissue, °C
T_b	arterial temperature, °C
T_i	initial temperature of tissue, °C
w_b	perfusion rate of blood, m^3/s/m^3

Greek symbols

λ	parameter defined in Eq. (20)
ρ	density, kg/m^3
ψ	volume fraction of magnetic particles
τ	relaxation time, s

Subscripts

i	node number
j	number of sub-space domain
k	number of layer
m	magnetic particle
t	tumor tissue

can solve the paradox of instantaneous responses of thermal disturbance occurred in the classical heat conduction equation, some studies [18–20] showed that the thermal wave model introduced some unusual behaviors and physically solutions. The rational thermal analysis is essential and helpful to the development of hyperthermia.

This work uses the dual-phase-lag (DPL) model to predict the temperature rise behavior in a two-layer concentric spherical region during magnetic tumor hyperthermia treatment. The DPL model describes a macroscopic temperature with the microstructural effect by introducing the phase lag times of heat flux and temperature gradient [21]. Antaki [22] has used the DPL model to interpret heat conduction in processed meat that was interpreted with the thermal wave model. From the measurement temperatures in Ref. [12], Antaki [22] predicted the phase lag time of heat flux to be 14–16 s and the phase lag time of temperature gradient to be 0.043–0.056 s for processed meat. Due to the geometry effect and the interfacial boundary conditions, the non-Fourier bio-heat transfer problem in a concentric spherical domain introduces the complexity and causes some mathematical difficulties. This work develops a hybrid numerical scheme based on the Laplace transform, change of variables, and the modified discretization technique in conjunction with the hyperbolic shape functions for solving the present problem. The similar method was used to solve various non-Fourier heat transfer problems and obtained the accurate results [23–25]. On the other hand, the metabolic heat generation rate and the blood perfusion rate may affect the temperature rise behavior in vivo during hyperthermia treatment. There exists the difference in metabolic heat generation rate, blood perfusion rate, and other physiological parameters between tumor and normal tissue [26–28]. It is a necessity to explore the influences of lag times, metabolic heat generation rate, blood perfusion rate, and other physiological parameters on the non-Fourier thermal response in tumor and health tissue for the present work.

2. Mathematical formulation

In a magnetic fluid hyperthermia, magnetic particles are injected into and homogenously distributed in a small tumor surrounded by the normal tissue. The small tumor is regarded as a solid sphere with the radius R [4–6] and becomes a heat source of constant power density P in the small tumor for excitation of alternating magnetic field. For $t > 0$, heat symmetrically transfers in the radius direction. The temperature distribution in the tumor ($0 \leqslant r \leqslant R$) and normal ($R \leqslant r \leqslant \infty$) tissues is the function of the distance r from the center of the sphere and time t. The present work explores the thermal behavior of DPL bio-heat transfer from this system.

The linearized form of the DPL model is based on the equation

$$\tau_q \frac{\partial q}{\partial t} + q = -k\frac{\partial T}{\partial r} - k\tau_T \frac{\partial^2 T}{\partial t \partial r} \tag{1}$$

where T is the temperature, k the heat conductivity, q the heat flux, t the time, and r the space variable. τ_q means the phase lag of the heat flux and τ_T means the phase lag of the temperature gradient. The heat flux precedes the temperature gradient for $\tau_q < \tau_T$. The temperature gradient precedes the heat flux for $\tau_q > \tau_T$. The DPL model depicts that not only the temperature gradient may precede the heat flux, but also the heat flux may precede the temperature gradient. In bio-heat transfer, Antaki [22] interpreted τ_q as a delay time for contact resistance between tissue particles. On the other hand, τ_T was interpreted as a measure of the conduction that occurs within tissues particles.

In a local energy balance, the one-dimensional energy equation of the present problem is given as

$$\rho c \frac{\partial T}{\partial t} = -\frac{\partial q}{\partial r} - \frac{2}{r} q + w_b \rho_b c_b (T_b - T) + q_m + q_r \tag{2}$$

where ρ, c, k, and T denote density, specific heat, thermal conductivity, and temperature in two regions. ρ_b, c_b, and w_b, respectively, are the density, specific heat, and perfusion rate of blood. q_m is the metabolic heat generation and only is a function of r in the present problem. The spatial heating source q_r is defined as $q_r = Pu(t)$, where $u(t)$ is a step function. T_b is the arterial temperature and is specified as 37 °C. The region $0 \leqslant r \leqslant R$ is a composite of tumor and magnetic particles. The effective density ρ_1 and the effective specific heat c_1 are calculated as $\rho_1 = \psi\rho_m + (1 - \psi)\rho_t$ and $c_1 = \psi c_m + (1 - \psi)c_t$, where subscripts m and t symbol the magnetic particles and the tumor tissue. ψ is the volume fraction of magnetic particles.

Substituting Eq. (1) into the energy conservation equation (2) leads to the heat transport equations in the tumor and normal tissues with constant physiological parameters as the following:

$$k_1\frac{1}{r^2}\frac{\partial}{\partial r}\left[r^2\left(\frac{\partial T_1}{\partial r}+\tau_{T1}\frac{\partial^2 T_1}{\partial t\partial r}\right)\right] = \left(1+\tau_{q1}\frac{\partial}{\partial t}\right)\left[\rho_1 c_1\frac{\partial T_1}{\partial t}-w_{b1}\rho_b c_b(T_b-T_1)-q_{m1}-q_{r1}\right] \quad \text{for } 0\leqslant r\leqslant R \tag{3}$$

$$k_2\frac{1}{r^2}\frac{\partial}{\partial r}\left[r^2\left(\frac{\partial T_2}{\partial r}+\tau_{T2}\frac{\partial^2 T_2}{\partial t\partial r}\right)\right] = \left(1+\tau_{q2}\frac{\partial}{\partial t}\right)\left[\rho_2 c_2\frac{\partial T_2}{\partial t}-w_{b2}\rho_b c_b(T_b-T_2)-q_{m2}\right] \quad \text{for } R\leqslant r\leqslant\infty \tag{4}$$

The present work regards the temperature and the heat flux at the interface of two regions is continuous. The boundary conditions are described as

$$\frac{\partial T_1(0,t)}{\partial r}=0 \quad \text{and} \quad T_1(0,t) \text{ is finite} \tag{5}$$

$$T_1(R,t)=T_2(R,t) \tag{6}$$

$$q_1(R,t)=q_2(R,t) \tag{7}$$

$$T_2(\infty,t)=T_i \tag{8}$$

and the initial conditions are

$$T_k(r,0)=T_i, \quad \frac{\partial T_k(r,0)}{\partial t}=0, \quad \text{and } q_k(r,0)=0 \qquad k=1,2 \tag{9}$$

where the subscript k is the number of layer. $k=1$ and $k=2$ mean the tumor and the normal tissue, respectively. The initial temperature T_i is regarded as the arterial temperature.

3. Numerical scheme

For convenience of analysis, a new dependent variable H is defined as

$$H=r(T-T_i) \tag{10}$$

The temperature difference, $T-T_i$, is equal to H/r. The value of H/r at $r=0$ is indeterminate and must be replaced by its limit as $r\to 0$. Thus the value of the transient temperature at the center, $T(0,t)$, is evaluated by using L'Hôspital's rule as

$$T(0,t)=\lim_{r\to 0}\frac{H}{r}+T_i=\frac{dH}{dr}+T_i \tag{11}$$

Under the circumstance, Eqs. (3) and (4) in terms of H for $T_i=T_b$ can be rewritten as

$$k_1\left(1+\tau_{T1}\frac{\partial}{\partial t}\right)\frac{\partial^2 H_1}{\partial r^2}=\left(1+\tau_{q1}\frac{\partial}{\partial t}\right)\left[\rho_1 c_1\frac{\partial H_1}{\partial t}+w_{b1}\rho_b c_b H_1 +(q_{m1}+q_{r1})r\right] \quad \text{for } 0\leqslant r\leqslant R \tag{12}$$

$$k_2\left(1+\tau_{T2}\frac{\partial}{\partial t}\right)\frac{\partial^2 H_2}{\partial r^2}=\left(1+\tau_{q2}\frac{\partial}{\partial t}\right)\left[\rho_2 c_2\frac{\partial H_2}{\partial t}+w_{b2}\rho_b c_b H_2+q_{m2}r\right] \quad \text{for } R\leqslant r\leqslant\infty \tag{13}$$

The boundary conditions and the initial conditions become

$$H_1(0,t)=0 \tag{14}$$

$$H_1(R,t)=H_2(R,t) \tag{15}$$

$$q_1(R,t)=q_2(R,t) \tag{16}$$

$$H_2(a,t)=0 \tag{17}$$

and

$$H_k(r,0)=0, \frac{\partial H_k(r,0)}{\partial t}=0, \quad \text{and } q_k(r,0)=0 \quad k=1,2 \tag{18}$$

Subsequently, the Laplace transform technique is used to map the transient problem into the steady one. The differential equations (12) and (13) are transformed under the initial conditions (18) as

$$\frac{d^2\tilde{H}_k}{dr^2}-\lambda_k^2\tilde{H}_k=-f_k r \tag{19}$$

where s is the Laplace transform parameter of time t. λ_k^2, f_1, f_2, and K_k are defined as

$$\lambda_k^2=\frac{1}{K_k}(\rho_k c_k s+w_b\rho_b c_b) \quad k=1,2 \tag{20}$$

$$f_1=\frac{q_{m1}+P(1+\tau_{q1}s)}{k_1(1+\tau_{T1}s)s} \tag{21a}$$

$$f_2=\frac{q_{m2}}{k_2(1+\tau_{T2}s)s} \tag{21b}$$

$$K_k=k_k\frac{1+\tau_{Tk}s}{1+\tau_{qk}s} \quad k=1,2 \tag{22}$$

In accordance with Eq. (1), the boundary conditions (14)–(17) in the Laplace transform domain can be written as

$$\tilde{H}_1(0,s)=0 \tag{23}$$

$$\tilde{H}_1(R,s)=\tilde{H}_2(R,s) \tag{24}$$

$$K_1\left(\frac{d\tilde{H}_1(R,s)}{dr}-\frac{\tilde{H}_1}{R}\right)=K_2\left(\frac{d\tilde{H}_2(R,s)}{dr}-\frac{\tilde{H}_2}{R}\right) \tag{25}$$

$$\tilde{H}_2(\infty,s)=0 \tag{26}$$

The present paper divides the whole space domain into several sub-space domains. For continuities of heat flux and temperature within the whole space domain, the following conditions are required at the interface of the sub-space domain $j-1$, $[r_{i-1},r_i]$, and the sub-space domain j, $[r_i,r_{i+1}]$.

$$\tilde{H}_{j-1,k}(r_i)=\tilde{H}_{j,k}(r_i) \quad i=1,2,\ldots,n;\ j=i;\ k=1,2 \tag{27}$$

$$K_k\left(\frac{d\tilde{H}_{j-1,k}(r_i)}{dr}-\frac{\tilde{H}_{j-1,k}}{r_i}\right)=K_k\left(\frac{d\tilde{H}_{j,k}(r_i)}{dr}-\frac{\tilde{H}_{j,k}}{r_i}\right) \quad i=1,2,\ldots,n;\ j=i;\ k=1,2 \tag{28}$$

where the subscript i is the number of node. n is the total number of nodes.

A modified discretization technique based on Eqs. (27) and (28) is developed for the governing algebraic equations in the present paper. Before performing the derivation of the governing algebraic equations, $\tilde{H}$ should be approximated by using the nodal temperatures and shape function within a small sub-space domain. It is a necessity to carefully choose he shape functions for the accuracy and stability of the numerical results [20]. Thus, the present work derives the shape functions from the governing equation (19).

For the sub-space domain j, $[r_i, r_{i+1}]$, the analytical solution of the governing equation (19) subjected to the boundary conditions

$$\tilde{H}_{j,k}(r_i)=\tilde{H}_{i,k} \quad \text{and} \quad \tilde{H}_{j,k}(r_{i+1})=\tilde{H}_{i+1,k} \tag{29}$$

are easily obtained and can be written as

$$\tilde{H}_{j,k}=\frac{1}{\sinh\lambda_k}\left\{\left(\tilde{H}_{i,k}-\frac{f_k}{\lambda_k^2}r_k\right)\sinh\lambda_k(r_{i+1}-r)+\left(\tilde{H}_{i+1,k}-\frac{f_k}{\lambda_k^2}r_{i+1}\right)\sinh\lambda_k(r-r_i)\right\}+\frac{f_k}{\lambda_k^2}r \tag{30}$$

Similarly, Eq. (25) in the sub-space domain $k-1$, $[r_{i-1}, r_i]$, can be written as

$$\tilde{H}_{j-1,k}=\frac{1}{\sinh\lambda_k}\left\{\left(\tilde{H}_{i-1,k}-\frac{f_k}{\lambda_k^2}r_{i-1}\right)\sinh\lambda_k(r_i-r)+\left(\tilde{H}_{i,k}-\frac{f_k}{\lambda_k^2}r_i\right)\sinh\lambda_k(r-r_{i-1})\right\}+\frac{f_k}{\lambda_k^2}r \tag{31}$$

where ℓ denotes the length of sub-space domain or the distance between two neighboring nodes. The value of ℓ can be different in the different layer.

Substituting Eqs. (27), (30), and (31) into Eq. (28) and then evaluating the resulting derivative can lead to the discretized form for the interior nodes in layer k as following

$$\tilde{H}_{i-1,k}-2\cosh(\lambda_k r)\tilde{H}_{i,k}+\tilde{H}_{i+1,k}=\frac{f_k}{\lambda_k^2}[r_{i-1}-2r_i\cosh(\lambda_k r)+r_{i+1}] \tag{32}$$

The discretized form for the node at the interface of the tumor and normal tissues, $r = R$, can be obtained from the boundary condition (25) and is written as

$$K_1\frac{\lambda_1}{\sinh\lambda_1\ell}\tilde{H}_{i-1,1}-\left(K_1\frac{\lambda_1\cosh\lambda_1\ell}{\sinh\lambda_1\ell}+K_2\frac{\lambda_2\cosh\lambda_2\ell}{\sinh\lambda_2\ell}+\frac{K_2}{R}-\frac{K_1}{R}\right)\tilde{H}_{i,(1,2)}+K_2\frac{\lambda_2}{\sinh\lambda_2\ell}\tilde{H}_{i+1,2}=K_1\frac{1}{\sinh\lambda_1\ell}\frac{f_1}{\lambda_1}(R-\ell)-\left(K_1\frac{\cosh\lambda_1\ell}{\sinh\lambda_1\ell}\frac{f_1}{\lambda_1}+K_2\frac{\cosh\lambda_2\ell}{\sinh\lambda_2\ell}\frac{f_2}{\lambda_2}\right)R+K_2\frac{1}{\sinh\lambda_2\ell}\frac{f_2}{\lambda_2}(R+\ell)+K_1\frac{f_1}{\lambda_1^2}-K_2\frac{f_2}{\lambda_2^2} \tag{33}$$

Eqs. (32) and (33) in conjunction with the discretized forms of the boundary conditions can be rearranged as the following matrix equation

$$[B]\{\tilde{H}\}=\{F\} \tag{34}$$

where $[B]$ is a matrix with complex numbers, $\{\tilde{H}\}$ is a column vector in the Laplace transform domain, and $\{F\}$ is a column vector representing the forcing term. Thereafter, the value of H in the physical domain can be determined with the application of the Gaussian elimination algorithm and the numerical inversion of the Laplace transform [29].

4. Results and discussion

The present results are for a small spherical tumor of radius $R = 0.00315$ m with a constant power density of 6.15×10^6 W/m^3 embedded in extended muscle tissue. The values of relevant thermal parameters are taken to be $k_1 = 0.778$ W/Km, $\rho_1 = 1660$ kg/m^3, $c_1 = 2540$ J/kgK, $k_2 = 0.642$ W/Km, $\rho_2 = 1000$ kg/m^3, and $c_2 = 3720$ J/kgK [4]. The metabolic heat generation rates of tumor and normal tissue are respectively determined as $q_{m1} = 29{,}000$ W/m^3 and $q_{m2} = 450$ W/m^3. The corresponding perfusion rates are $w_{b1} = 0.009$ m^3/s/m^3 and $w_{b2} = 0.00018$ m^3/s/m^3 [14]. The volumetric heat capacity of blood is $\rho_b c_b = 4.18\times10^6$ J/m^3/K [6]. Some parameter values are possibly adjusted for comparison and discussion and are noted in each figure. The phase lag times determined by Antaki [22] based on the measured temperatures of Mitra et al. [12] become the reference values of τ_q and τ_T. All the computations are performed with the uniform space size $\ell = R/100$.

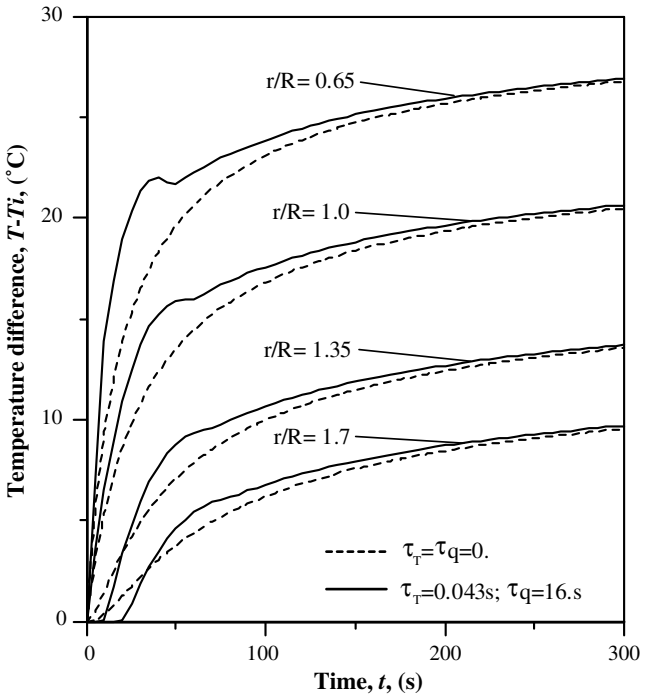

Fig. 1. Variation of temperature at different reduced distance r/R from the center for $\tau_T = \tau_q = 0$ and $\tau_T = 0.043$ s and $\tau_q = 16$ s.

Fig. 1 presents the variation of temperature at different reduced distance r/R from the center for $\tau_T = \tau_q = 0$ (i.e., $\tau_{T1} = \tau_{T2} = 0$; $\tau_{q1} = \tau_{q2} = 0$) and for $\tau_T = 0.043$ s (i.e., $\tau_{T1} = \tau_{T2} = 0.043$ s) and $\tau_q = 16$ s (i.e., $\tau_{q1} = \tau_{q2} = 16$ s). As $\tau_T = \tau_q = 0$, the Pennes' equation can describe the behavior of bio-heat transfer. The thermal response is extremely fast at the locations $r/R = 0.65$, 1.0, 1.35, and 1.7 for the infinite propagation velocity of thermal signal, and the temperatures gradually rise with time for the continuous heating. As $\tau_T = 0.043$ s and $\tau_q = 16$ s, the non-Fourier effect is obvious in the behavior of bio-heat transfer. Since the locations $r/R = 1.35$ and $r/R = 1.7$ are out of the range of heating source, the thermal signal reaches them needs a period. The finite propagation effect also makes the curves of temperature variation wave. The waving phenomenon is more obvious near the heating source. The predicted temperatures from the equation for the dual-phase-lag model of bio-heat transfer are higher than those from the Pennes' equation during $0 < t < 200$ s. After that, the predicted temperatures approach consistence for $\tau_T = \tau_q = 0$ and $\tau_T = 0.043$ s and $\tau_q = 16$ s. The above results reflect that the dual-phase-lag model accounts the effects of local non-equilibrium on the thermal behavior at the early times of heating.

The metabolic heat generation and blood perfusion rates are important characteristics of living tissues. In accordance with Refs. [27,28], the metabolic heat generation and blood perfusion rates are different between tumor and normal tissue. However, Maenosono and Saita [6] regarded their same values for tumor and normal tissue. Andrä et al. [4] predicted the temperature distribution in breast with neglecting the effects of blood perfusion and metabolism. Obviously, the metabolic heat generation rate and the blood perfusion rate are not uncertainties. This difference may significantly affect the temperature rise during a hyperthermia treatment. The present work explores the effect of the metabolic heat generation rate on the non-Fourier bio-heat transfer, as shown in Fig. 2, in which presents the temperature distributions

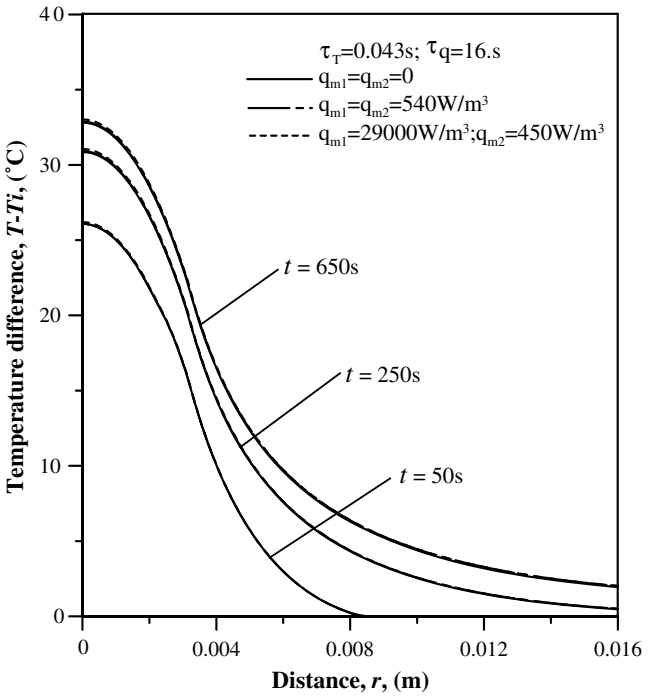

Fig. 2. Effect of the metabolic heat generation rate on the non-Fourier bio-heat transfer.

for $q_{m1} = q_{m2} = 0$, $q_{m1} = q_{m2} = 540\ \mathrm{W/m^3}$, and $q_{m1} = 29{,}000\ \mathrm{W/m^3}$ and $q_{m2} = 450\ \mathrm{W/m^3}$ at various times. The temperatures are higher in the domain occupied by the heat source. For heat diffusing, the affected domain increases with time, but the rising rate of temperature becomes slow. Further, it is observed from Fig. 2 that the temperature distributions of these three cases are very similar. The metabolic heat generation rate seems not to affect the non-Fourier behavior of bio-heat transfer in the present problem.

Fig. 3 presents the history of thermal response at various locations for $w_{b1} = w_{b2} = 0.0064\ \mathrm{m^3/s/m^3}$, which was used by Maenosono and Saita [6] to estimate the temperature rise behavior in vivo with solving the Pennes' equation. The blood perfusion plays the cooling role, while the temperature of blood is regarded as the constant temperature 37 °C. As the difference between the tumor and blood temperatures is not large enough yet, the amount of heat loss through the blood perfusion is small and the cooling function is not obvious. Correspondingly, as the difference between the tissue and blood temperatures is enlarged, the heat loss through the blood perfusion increases and slows down the rising rate of temperature, as shown in Fig. 3. It is possible that the temperature distribution in the tissues comes to the steady status for the cooling effect of the blood perfusion. The comparison of Fig. 3 with Fig. 1 shows that the blood perfusion rate changes from $w_{b1} = 0.009\ \mathrm{m^3/s/m^3}$ and $w_{b2} = 0.00018\ \mathrm{m^3/s/m^3}$ to $w_{b1} = w_{b2} = 0.0064\ \mathrm{m^3/s/m^3}$ does not affect the behavior of thermal wave, but able to adjust the tissue temperature.

For high Curie temperature, high saturation magnetization, and high chemical stability, FePt magnetic nanoparticles (MNPs) are used for magnetic hyperthermia. Maenosono and Saita [6] presented that 9-nm fcc FePt MNPs can dissipate the energy $p = 3.97 \times 10^5\ \mathrm{W/m^3}$ in the magnetic field that amplitude and frequency are fixed at 50 mT and 300 kHz for the volume fraction $\psi = 2 \times 10^{-5}$. Fig. 4 illustrates the transient temperatures at the locations $r/R = 0.65$, 1.0, 1.35, and 1.7 for $q_{m1} = q_{m2} = 540\ \mathrm{W/m^3}$ and $p = 3.97 \times 10^5\ \mathrm{W/m^3}$. It is found that the curves in Fig. 4 are similar to those in Fig. 1, except the values of the temperature difference $T - T_i$. The proportion of the temperature value in Fig. 1 to that in Fig. 4 almost equals to $6.15 \times 10^6\ \mathrm{W/m^3}/3.97 \times 10^5\ \mathrm{W/m^3}$. This phenomenon implies that the cooling function of blood perfusion does not efficiently work as $w_{b1} = 0.009\ \mathrm{m^3/s/m^3}$ and $w_{b2} = 0.00018\ \mathrm{m^3/s/m^3}$. Also, $540\ \mathrm{W/m^3}$ and $450\ \mathrm{W/m^3}$ compared to $6.15 \times 10^6\ \mathrm{W/m^3}$ and $3.97 \times 10^5\ \mathrm{W/m^3}$ are very small, so the effect of the metabolic heat generation on the temperature rise can be ignored.

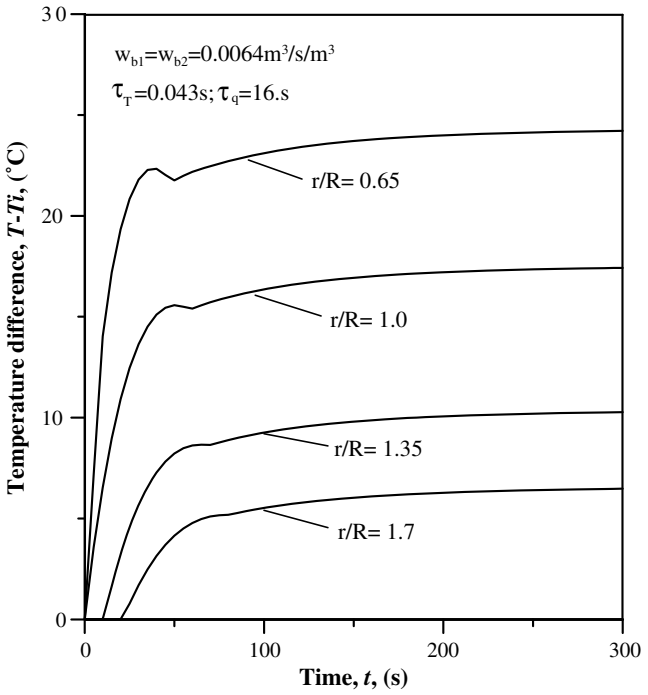

Fig. 3. History of thermal response at various locations for $w_{b1} = w_{b2} = 0.0064\ \mathrm{m^3/s/m^3}$.

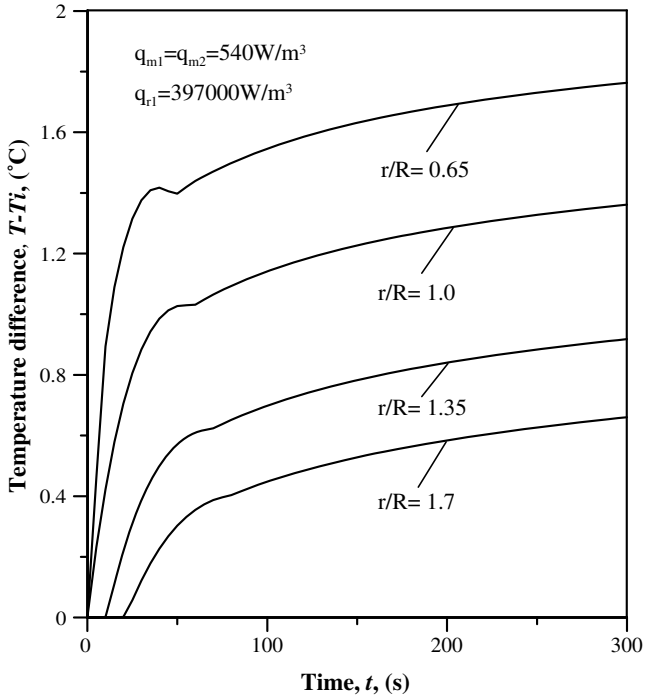

Fig. 4. Transient temperatures at the locations $r/R = 0.65$, 1.0, 1.35, and 1.7 for $q_{m1} = q_{m2} = 540\ \mathrm{W/m^3}$ and $p = 3.97 \times 10^5\ \mathrm{W/m^3}$.

The lag times, τ_q and τ_T, are the characteristic of the dual-phase-lag model. To explore the effects of τ_q and τ_T on the bio-heat transfer, Fig. 5 shows the history of thermal response at the locations $r/R = 1.0$, 1.5, and 2.5 for $\tau_T = 0.0215$ s and $\tau_q = 8$ s, $\tau_T = 0.043$ s and $\tau_q = 16$ s, and $\tau_T = 0.0645$ s and $\tau_q = 24$ s. It is observed from Fig. 5 that these three sets of τ_q and τ_T, which have the same τ_T/τ_q value, do not get the same behavior of temperature rise. In other words, the total effect of τ_q and τ_T on the bio-heat transfer may be different for the same τ_T/τ_q value. Since the location $r/R = 1.0$ is within the range of heating source, the thermal response is not delay there. The thermal delay appears at the locations $r/R = 1.5$ and 2.5, and the delay time is proportional to the distance from the center of tumor. It shows the behavior of finite propagation of thermal signal. In accordance with the contents of the literatures [21,24,30], it is known that the lag time τ_q can dominate the behavior of thermal wave propagation, slow down the propagation velocity of thermal signal, and manifest the feature of thermal wave. Due to the effect of τ_T, the characters of thermal wave would decay in DPL heat transfer. As $\tau_T = 0.0645$ s and $\tau_q = 24$ s, the propagation velocity is slower, but the feature of thermal wave is obvious. Probably, the effect of $\tau_q = 24$ s on the present problem is over the effect of $\tau_T = 0.0645$ s. On the other hand, the thermal wave propagation is gradually replaced by the diffusion behavior with the penetration distance of thermal signal increasing. With time passing over, the local temperature approaches the same for the present three sets of τ_q and τ_T. This phenomenon demonstrates that the lag times, τ_q and τ_T, affect the bio-heat transfer only at the early times of heating.

Further, to know the effect of τ_T on the bio-heat transfer, Fig. 6 presents the variation of thermal response at $r/R = 1.5$ for $\tau_q = 16$ s and various values of τ_T. It is found that increasing the value of τ_T can shorten the time which the thermal signal reaches the location $r/R = 1.5$. This result implies that the effect of τ_T can assist heat energy diffuse. The affected degree is proportional to the value of τ_T. As $\tau_T = 3$ s, the behavior of thermal wave decays at a faster rate and the temperature variation curve becomes smoother. The lag time τ_T reflects the micro-structural interaction effect in the media of heat transfer [21]. In other words, the micro-structural interaction effect can significantly extend the physical domain of the thermal penetration depth.

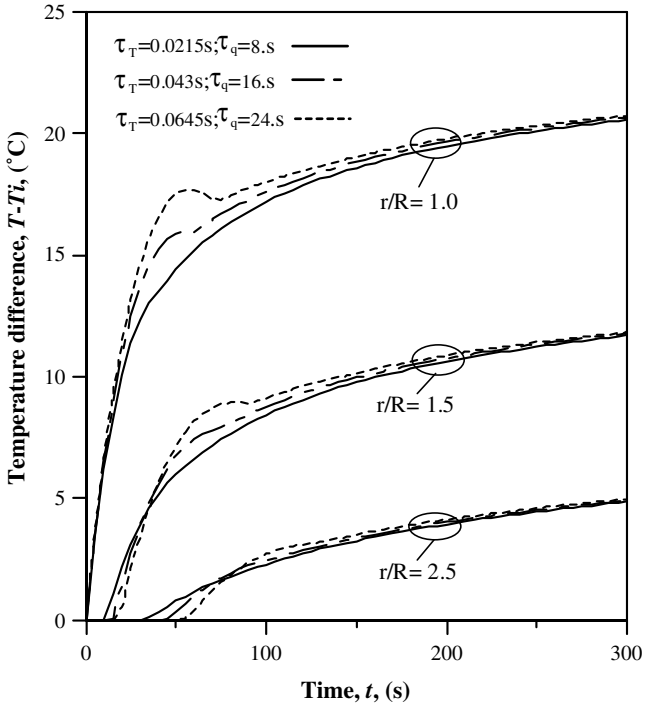

Fig. 5. History of thermal response at the locations $r/R = 1.0$, 1.5, and 2.5 for various sets of τ_T and τ_q.

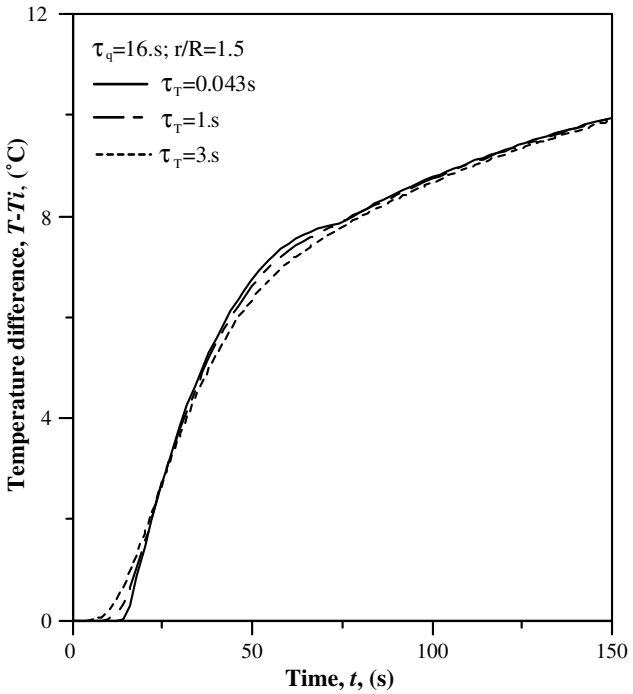

Fig. 6. Variation of thermal response at $r/R = 1.5$ for $\tau_q = 16$ s and various values of τ_T.

The values of τ_q and τ_T may be different in tumor and normal tissue as well as the other physiological parameters. For comparison and discussion, the present work assumes two sets of τ_q and τ_T. The first set is $\tau_{T1} = 0.043$ s; $\tau_{q1} = 24$ s and $\tau_{T2} = 0.056$ s; $\tau_{q2} = 14$ s, and the other is $\tau_{T1} = 0.056$ s; $\tau_{q1} = 14$ s and $\tau_{T2} = 0.043$ s; $\tau_{q2} = 24$ s. Fig. 7 plots the temperature distributions at $t = 50$ s, 250 s, and 650 s for these two sets of τ_q and τ_T. From the results shown in Figs. 5 and 6, it is known that the ability of heat transfer in the media increases with the value of τ_T, but not with the value of τ_q. As $\tau_{T2} = 0.056$ s and $\tau_{q2} = 14$ s, heat energy can be transported away from the interface of the tumor and normal tissue at a faster velocity. Therefore, the tumor temperature for the first set of τ_q and τ_T is lower than that for the other set at $t = 50$ s, but the affected domain is larger. As $t = 250$ s, the effects of the difference in the lag times between the tumor and normal tissue on the temperature distribution nearly disappear, and two temperature distribution curves almost coincide in the domain $0 \leqslant r \leqslant 0.016m$. At $t = 650$ s, the temperature distribution curves are completely consistent. It further shows that the behavior of non-Fourier bio-heat transfer is concerned with the lag times only at the early stages of heating.

Fig. 8 presents the temperature distributions with $w_{b1} = w_{b2} = 0.0064\ m^3/s/m^3$ at various times for $\tau_{Ti} = 0.056$ s; $\tau_{q1} = 14$ s and $\tau_{T2} = 0.043$ s; $\tau_{q2} = 24$ s. The comparison between Figs. 7 and 8 shows that the blood perfusion rate can dominate the temperature distribution. In substance, the amount of heat loss through the blood depends on the perfusion rate. At $t = 50$ s, the most part of heat energy still accumulates in the tumor domain, thus the tumor temperature for $w_{b1} = 0.0064\ m^3/s/m^3$ is slightly higher than that for $w_{b1} = 0.009\ m^3/s/m^3$, as shown in Fig. 7. When the blood perfusion rate in the normal tissue increases from $w_{b2} = 0.00018\ m^3/s/m^3$ to $w_{b2} = 0.0064\ m^3/s/m^3$, the cooling ability of the whole

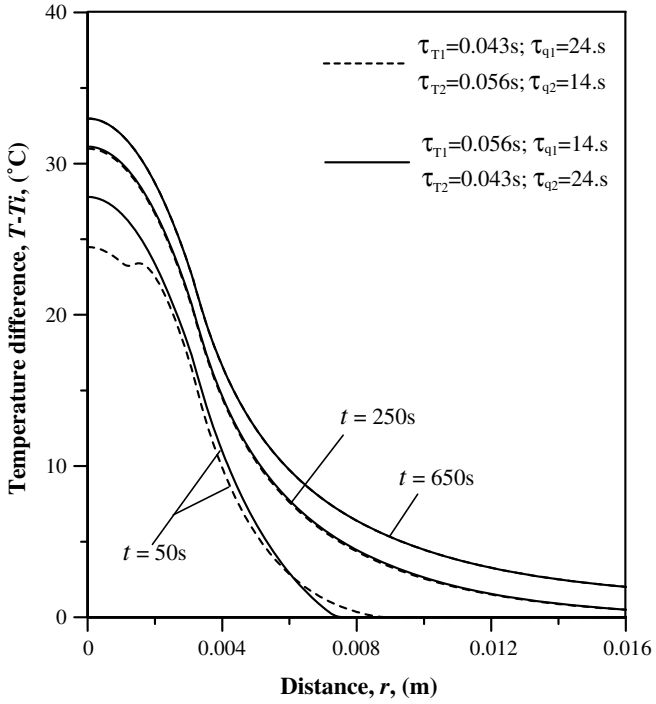

Fig. 7. Effect of the difference in τ_q and τ_T between the tumor and normal tissue.

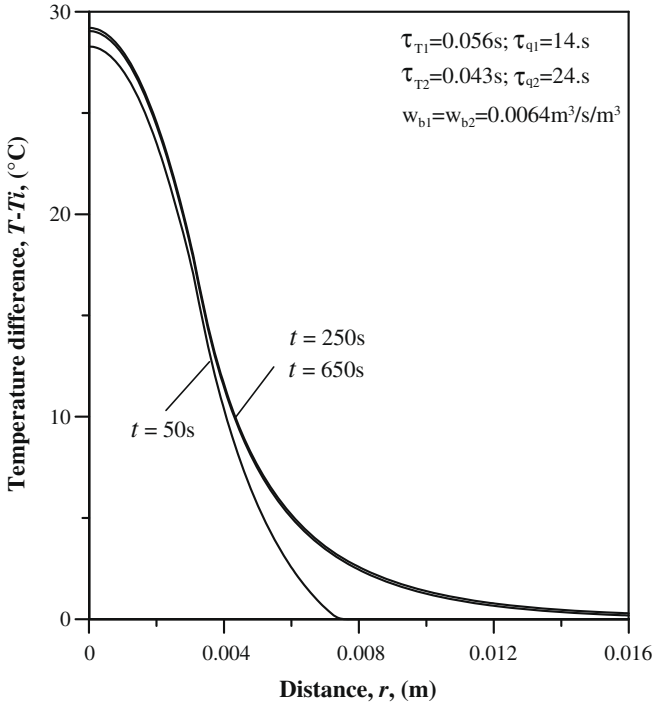

Fig. 8. Temperature distributions with $w_{b1} = w_{b2} = 0.0064\ m^3/s/m^3$ at various times for $\tau_{T1} = 0.056$ s; $\tau_{q1} = 14$ s and $\tau_{T2} = 0.043$ s; $\tau_{q2} = 24$ s.

domain is enhanced. With time passing, the heat loss through the blood perfusion increases. Then the rate of temperature rise tends to be gradual. As $t = 250$ s, the temperature distribution is nearly steady. Judging from this, the blood perfusion rate can control the tumor temperature and the affected domain. In other words, the control of the blood perfusion rate is helpful to have an ideal hyperthermia treatment, which should selectively destroy the tumor cells without damaging the surrounding healthy tissue.

Fig. 9 presents the variation of $T - T_i$ at $r = 0$ for various sets of τ_T and τ_q. Though the location $r = 0$ is a singular point in this problem, the present numerical results are stable and have the finite value. It presents that the present numerical scheme is stable for analyzing such problems. For $\tau_T = \tau_q = 0$, the temperature smoothly rises with

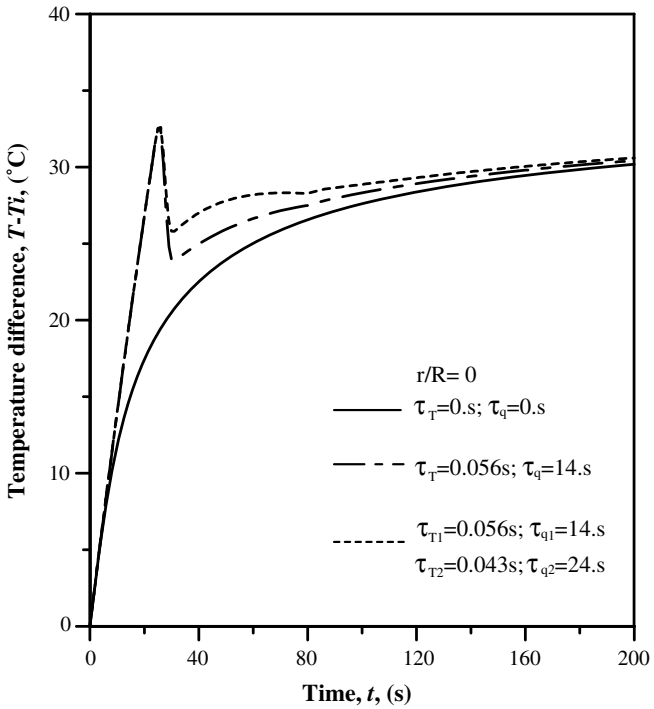

Fig. 9. Variation of $T - T_i$ at $r = 0$ for various sets of τ_T and τ_q.

time and approaches to the status of thermal equilibrium at $r = 0$. The behavior of thermal wave is obvious and gradually reduces with time for $\tau_T = 0.056$ s; $\tau_q = 14$ s and $\tau_{T1} = 0.056$ s; $\tau_{q1} = 14$ s and $\tau_{T2} = 0.043$ s; $\tau_{q2} = 24$ s. Due to the difference of the physiological parameters, the internal reflection and transmission occur at the interface of the tumor and normal tissue. The reflected thermal pulses move toward the center of tumor $r = 0$ and make the temperature sharply vary. In the case of $\tau_{T1} = 0.056$ s; $\tau_{q1} = 14$ s and $\tau_{T2} = 0.043$ s; $\tau_{q2} = 24$ s, the ability of heat transfer of the normal tissue is reduced for the effect of the lag times. Heat energy is more difficult to be transferred away from the interface. Thus the temperature drops down at a slower rate. It means that decreasing the value of τ_q can increase the ability of heat transfer in the media. Actually, the other thermal properties can also affect energy passing through the interface [24,30].

5. Conclusions

The behavior of bio-heat transfer in multi-layer living tissues with the non-Fourier effect is studied during magnetic hyperthermia. A hybrid numerical scheme based on the Laplace transform, change of variables, and the modified discretization technique in conjunction with the hyperbolic shape functions is extended to solve the non-Fourier bio-heat transfer problem in spherical coordinate system. The influences of lag times, metabolic heat generation rate, blood perfusion rate, and other physiological parameters on the non-Fourier thermal response in tumor and normal tissue are discussed.

While the metabolic heat generation takes little percentage of heating source, its effect on the temperature rise can be ignored. The cooling effect of the blood perfusion can control the tumor temperature and the affected domain. The control of the blood perfusion rate is helpful to have an ideal hyperthermia treatment. It is known that the lag time τ_q can dominate the behavior of thermal wave propagation, slow down the propagation velocity of thermal signal, and manifest the feature of thermal wave. The effect of τ_T can assist heat energy diffuse and make the characters of thermal wave decay in DPL heat transfer. However, the total effect of τ_q and τ_T on the bio-heat transfer may be different for the same τ_T/τ_q value. Actually, the behavior of non-Fourier bio-heat transfer is concerned with the lag times only at the early stages of heating. The lag time τ_T reflects the micro-structural interaction effect in the media. In other words, the micro-structural interaction effect can significantly affect the transient behavior of bio-heat transfer in living tissues.

However, the lag times, the metabolic heat generation rate and the blood perfusion rate are not uncertainties. The experiment to further know these effects is needed.

References

[1] W.C. Dewey, D.E. Thrall, E.L. Gillette, Hyperthermia and radiation – selective thermal effect on chronically hypoxic tumor-cells in vivo, Int. J. Radiat. Oncol. Biol. Phys. 99 (1977) 99–103.
[2] P. Moroz, S.K. Jones, B.N. Gray, Magnetically mediated hyperthermia: current status and future directions, Int. J. Hyperthermia 18 (2002) 267–284.
[3] J.J.W. Lagendijk, Hyperthermia treatment planning, Phys. Med. Biol. 45 (2000) R61–R76.
[4] W. Andrä, C.G. d'Ambly, R. Hergt, I. Hilger, W.A. Kaiser, Temperature distribution as function of time around a small spherical heat source of local magnetic hyperthermia, J. Magn. Magn. Mater. 194 (1999) 197–203.
[5] H.G. Bagaria, D.T. Johnson, Transient solution to the bioheat equation and optimization for magnetic fluid hyperthermia treatment, Int. J. Hyperthermia 21 (2005) 57–75.
[6] S. Maenosono, S. Saita, Theoretical assessment of FePt nanoparticles as heating elements for magnetic hyperthermia, IEEE Trans. Magnetics 42 (2006) 1638–1642.
[7] J.W. Durkee, P.P. Antich, C.E. Lee, Exact solutions to the multiregion time-depedent bioheat equation. I: solution development, Phys. Med. Biol. 35 (1990) 847–867.
[8] N. Tsuda, K. Kuroda, Y. Suzuki, An inverse method to optimize heating conditions in RF-capacitive hyperthermia, IEEE. Trans. Biomed. Eng. 43 (1996) 1029–1037.
[9] A.V. Luikov, Analytical Heat Diffusion Theory, Academic Press, New York, 1968.
[10] W. Kaminski, Hyperbolic heat conduction equation for material with a non-homogenous inner structure, ASME J. Heat Transfer 112 (1990) 555–560.
[11] A.M. Braznikov, V.A. Karpychev, A.V. Luikova, One engineering method of calculating heat conduction process, Inzhenerno Fizicheskij Zhurnal 28 (1975) 677–680.
[12] K. Mitra, S. Kumar, A. Vedavarz, M.K. Moallemi, Experimental evidence of hyperbolic heat conduction in processed meat, ASME J. Heat Transfer 117 (1995) 568–573.
[13] W. Roetzel, N. Putra, S.K. Das, Experiment and analysis for non-Fourier conduction in materials with non-homogeneous inner structure, Int. J. Therm. Sci. 42 (2003) 541–552.
[14] C. Cattaneo, Sulla conduzione de Calore, Atti del Semin. Mat. E Fis. Univ. Modena 3 (1948) 3–21.
[15] P. Vernotte, Les Paradoxes de la Theorie Continue de L'equation de la Chaleur, Compute Rendus 246 (1958) 3154–3155.
[16] H.D. Weymann, Finite speed of propagation in heat conduction, diffusion, and viscous shear motion, Am. J. Phys. 35 (1967) 488–496.
[17] S.L. Sobolev, Transport processes and traveling waves in systems with local non-equilibrium, Sov. Phys. Usp. 34 (1991) 217–229.
[18] Y. Taitel, On the parabolic, hyperbolic, and discrete formulation of the heat conduction equation, Int. J. Heat Mass Transfer 15 (1971) 369–371.
[19] C. Körner, H.W. Bergman, The physical defects of the hyperbolic heat conduction equation, Appl. Phys. A 67 (1998) 397–401.
[20] S. Godoy, L.S. García-Colín, Nonvalidity of the telegrapher's diffusion equation in two and three dimensions for crystalline solids, Phys. Rev. E 55 (1997) 2127–2131.
[21] D.Y. Tzou, Macro- to Microscale Heat Transfer: The Lagging Behavior, Taylor & Francis, Washington, DC, 1996.
[22] P.J. Antaki, New interpretation of non-Fourier heat conduction in processed meat, ASME J. Heat Transfer 127 (2005) 189–193.
[23] K.C. Liu, Analysis of thermal behavior in multi-layer metal thin-films based on hyperbolic two-step model, Int. J. Heat Mass Transfer 50 (2007) 1397–1407.
[24] K.C. Liu, Numerical analysis of dual-phase-lag heat transfer in a layered cylinder with nonlinear interface boundary conditions, Comput. Phys. Commun. 177 (2007) 307–314.
[25] K.C. Liu, Thermal propagation analysis for living tissue with surface heating, Int. J. Thermal Sci. 47 (2008) 507–513.
[26] C.W. Song, J.G. Rhee, S.H. Levitt, Blood flow in normal tissues and tumors during hyperthermia, J. Natl. Canc. Inst. 64 (1980) 119–124.
[27] M. Gautheric, Thermopathology of breast cancer: measurement and analysis of in vivo temperature and blood flow, Ann. N.Y. Acad. Sci. 335 (1980) 383–415.
[28] L. Hu, A. Gupta, J.P. Gore, L.X. Xu, Effect of forced convection on the skin thermal expression of breast cancer, ASME J. Heat Transfer 126 (2004) 204–211.
[29] G. Honig, U. Hirdes, A method for the numerical inversion of Laplace transforms, J. Comp. Appl. Math. 10 (1984) 113–132.
[30] K.C. Liu, P.J. Cheng, Numerical analysis for dual-phase-lag heat conduction in layered films, Numer. Heat Transfer A 49 (2006) 589–606.